

Uncertainty in Temperature-Based Determination of Time of Death

Martin Weiser · Bodo Erdmann ·
Sebastian Schenkl · Holger Muggenthaler ·
Michael Hubig · Gita Mall · Stefan Zachow

accepted 2018-03-12

Abstract Temperature-based estimation of time of death (ToD) can be performed either with the help of simple phenomenological models of corpse cooling or with detailed mechanistic (thermodynamic) heat transfer models. The latter are much more complex, but allow a higher accuracy of ToD estimation as in principle all relevant cooling mechanisms can be taken into account.

The potentially higher accuracy depends on the accuracy of tissue and environmental parameters as well as on the geometric resolution. We investigate the impact of parameter variations and geometry representation on the estimated ToD. For this, numerical simulation of analytic heat transport models is performed on a highly detailed 3D corpse model, that has been segmented and geometrically reconstructed from a computed tomography (CT) data set, differentiating various organs and tissue types. From that and prior information available on thermal parameters and their variability, we identify the most crucial parameters to measure or estimate, and obtain an a priori uncertainty quantification for the ToD.

This is a post-peer-review, pre-copyedit version of an article published in Heat and Mass Transfer. The final authenticated version is available online at: <http://dx.doi.org/10.1007/s00231-018-2324-4>.

Martin Weiser
Zuse Institute Berlin, Takustr. 7, 14195 Berlin, Germany, E-mail: weiser@zib.de

Bodo Erdmann
Zuse Institute Berlin

Sebastian Schenkl
Institute of Forensic Medicine, Jena University Hospital – Friedrich Schiller University, Jena, Germany

Holger Muggenthaler
Institute of Forensic Medicine

Michael Hubig
Institute of Forensic Medicine

Gita Mall
Institute of Forensic Medicine

Stefan Zachow
Zuse Institute Berlin

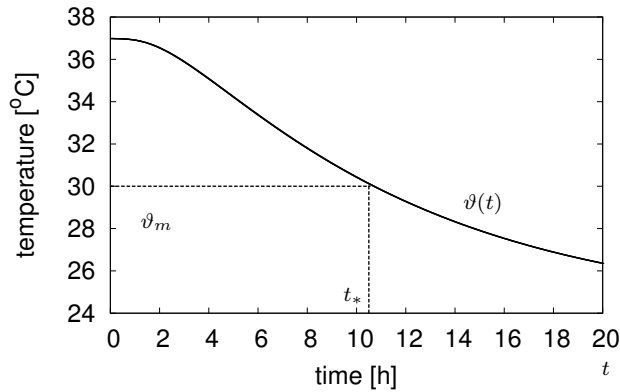


Fig. 1 Temperature-based estimation of the ToD. The intersection of a temperature curve $\vartheta(t)$ describing body cooling, with the horizontal line of a measured temperature ϑ_m yields the ToD estimate t_* . The overall qualitative shape of the cooling curve is characteristic for rectal measurement and the same for almost all corpses and environmental conditions.

Keywords time of death; forensic medicine; heat equation; sensitivity; geometric resolution; thermal parameters

1 Introduction

In the context of law enforcement in homicides, the use of temperature-based estimation of time of death (ToD) is of utmost importance. Such estimations are typically based on a single temperature measurement taken in the rectum. The intersection of a post-mortem rectal temperature-time curve $\vartheta(t)$ with the measured temperature ϑ_m provides an estimate $t_* = \vartheta^{-1}(\vartheta_m)$ of the ToD, see Figure 1.

For an accurate estimation of the ToD, the post-mortem temperature curves are crucial. Two different methods for defining these curves are conceivable: First, a phenomenological approach (PA), describing the temperature by parametrized arithmetic expressions. Marshall and Hoare [25] proposed a family of double-exponential curves with four parameters. This model, with empirical parameter definitions by Henßge [14] in terms of body weight and environmental temperature, has found widespread use in practical forensic work. The main drawback of the PA is its limited applicability to non-standard situations like irradiation from external sources, individually varying anatomy, or partial thermal insulation.

Second, a thermodynamic or mechanistic approach (MA), computing the temperature curve by a detailed simulation of the physical processes of heat transfer. Aiming at a faithful representation of the physical situation, the MA in principal allows a higher accuracy of ToD estimation as it can take all relevant heat transfer mechanisms into account, also those of non-standard situations. The reliability of the estimation depends on the accuracy of the physical model parameters such as corpse geometry and posture, tissue heat capacity and conductivity, and environmental conditions. While

mechanistic models contain many more parameters than phenomenological models, their parameters have a particular physical meaning and are, at least in principle, accessible to measurements. The main drawbacks of the MA are first the effort required to set up a specific computational model and second the lack of accurate parameter values in concrete situations.

Mall et al. [22,23] introduced a finite element (FE) based method for the simulation of corpse cooling, with a rather coarse corpse geometry and thermal tissue parameters taken from literature, and applied it to several cases of forensic practice. Already this approach provided estimates of ToD as good as or even more accurate than those obtained from the PA method [22,23].

In between these two different approaches are methods based on a physical heat transport model, but up to now employing more or less coarse approximations. Attempts at validation of such models have been presented by Smart [33] and Rodrigo [29,30].

In this paper we investigate the required accuracy of thermal model parameters and geometry in the MA that is needed for a sufficient accuracy of ToD estimation. In particular, we derive sensitivities of the estimated ToD with respect to various parameters. In Section 2, the FE-based method is briefly described. The influence of tissue and environmental parameters is analysed in Section 3, based on a highly detailed anatomical model that has been derived from CT data, differentiating several organs and tissue types.

Notation. For reference, the symbols used throughout the paper and their meaning are listed in Table 1.

2 Finite Element-based Method

Thermal model. The physical model of corpse cooling describes the temperature distribution ϑ by Fourier's law of heat conduction,

$$c\rho\dot{\vartheta} = \operatorname{div}(\kappa\nabla\vartheta) + Q, \quad (1)$$

where c is the specific heat capacity, ρ the density, and κ the heat conductivity of the tissue. The supravital metabolic heat generation Q continues for some hours after time of death, decreasing with the loss of oxygen supply and the decrease of tissue temperature. Its value $Q(t) = Q_0 \exp(-0.00024 \text{ s}^{-1} t)$ is assumed to decline exponentially from the initial value Q_0 with a half-value period of about 30 min.

We interpret the heat capacity $c\rho$ as a single parameter instead of treating density and specific heat capacity separately.

Heat transfer from the body to the environment across the boundary (skin) is due to conduction/advection and radiation:

$$n^T \kappa \nabla \vartheta = h(\vartheta_{\text{env}} - \vartheta) + \varepsilon \sigma (\vartheta_{\text{amb}}^4 - \vartheta^4) + \varepsilon q. \quad (2)$$

Here, n is the unit outer normal and h the heat transfer coefficient, ϑ_{env} the environmental temperature, ε the emissivity, ϑ_{amb} the perceived ambient radiative temperature, and $\sigma = 5.6704 \times 10^{-8} \text{ W m}^{-2} \text{ K}^{-4}$ the Stefan-Boltzmann constant. q is the external irradiation which we don't consider in this paper.

symbol	meaning	defined in
c	specific heat capacity of tissue	Tab. 2
$\rho_b c_b$	blood heat capacity	Tab. 3
γ	effective heat transfer coefficient	Tab. 3
δt	time deviation	eq. (6)
δp	parameter deviation	eq. (6)
ϵ	surface emissivity	Tab. 3
h	convective heat transfer coefficient	Tab. 3
I_x	impact of parameter x on time of death estimate	eq. (9)
\hat{I}_x	importance of parameter x	eq. (11)
κ	tissue heat conductivity	Tab. 2
n	surface outer unit normal	eq. (2)
n_p	number of parameters in the cooling model	p. 7
Ω	spatial domain occupied by the corpse	p. 5
p	parameters of the analytic cooling model	p. 7
\bar{p}	deviating parameter vector	eq. (6)
q	external irradiation	eq. (2)
Q	supravital metabolic heat	eq. (1)
Q_0	initial value of Q	p. 2
ρ	tissue density	Tab. 2
σ	Stefan-Boltzmann constant	eq. (2)
σ_x	standard deviation of quantity x	Tabs. 2 and 3
S	sensitivity vector of time of death estimate w.r.t. parameters	eq. (8)
t	time	
t_*	time of death (estimate)	p. 2
\tilde{t}	deviating time of death estimate	eq. (6)
ϑ	body temperature distribution	eq. (1)
$\vartheta(t; p)$	rectal cooling curve (that may depend on parameters)	p. 1
ϑ_0	vital temperature distribution	eq. (4)
ϑ_{amb}	ambient radiative temperature	eq. (3)
ϑ_{core}	vital body core temperature	eq. (4)
ϑ_{env}	environmental temperature	eq. (5)
$\dot{\vartheta}_{\text{env}}$	environmental temperature rate	Tab. 3
ϑ_m	measured rectal temperature	p. 2
V_x	volume fraction of tissue x	p. 15
w	tissue perfusion	Tab. 2

Table 1 Symbols used throughout the paper.

Several simulations have shown that in the usual range of temperatures (270 K to 310 K) a linearization of the Stefan-Boltzmann radiation term has a negligible impact on the cooling curve and hence on the estimated ToD. For the current study, we moreover assume $\vartheta_{\text{amb}} = \vartheta_{\text{env}}$, and therefore use the boundary condition

$$n^T \kappa \nabla \vartheta = \gamma (\vartheta_{\text{env}} - \vartheta) \quad (3)$$

with the effective heat transfer coefficient $\gamma = h + 4\epsilon\sigma\vartheta_{\text{env}}^3$.

The initial temperature field $\vartheta_0 = \vartheta(t)$ at time $t = 0$ is given by the vital temperature distribution and assumed to satisfy the Bio-Heat-Transfer-Equation (BHTE) due to Pennes [27],

$$-\text{div}(\kappa \nabla \vartheta_0) + \rho_b c_b w (\vartheta_0 - \vartheta_{\text{core}}) = 0, \quad (4)$$

where $\rho_b c_b$ is the heat capacity of blood, w the tissue perfusion, and ϑ_{core} the body core temperature.

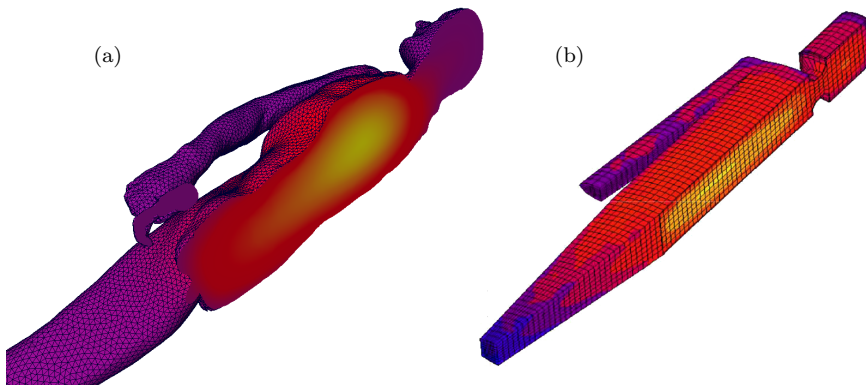


Fig. 2 Typical temperature distribution on different corpse models. (a): Fine tetrahedral mesh of a corpse’s geometry (including organs and other tissues) obtained from CT data by segmentation and geometry reconstruction. (b): Half of a symmetric but coarse corpse model as developed by [22] with color coded visualization of computed temperature distribution.

Anatomical model. The heat equation (1) is defined on a geometric domain $\Omega \subset \mathbb{R}^3$ representing the corpse. Of course, the temperature profile and hence the cooling curve depend on the size and shape of Ω . Moreover, the material parameters $c\rho$, κ , and w are different for various biological tissues, in particular muscle, adipose tissue, and bone. Thus, the cooling curve depends also on the size, shape, and position of different organs and tissue regions. For these reasons, a corpse model that contains those organs and represents the individual anatomy might be necessary for a sufficient accuracy of ToD estimation.

The invasive, direct detection of tissue components (mass, volume, and position) during post-mortem dissection can only be performed with great effort [5]. An alternative indirect quantitative capture of various tissue types based on medical imaging is difficult, takes higher efforts, but can be done with high accuracy in volume identification. Of course, this method doesn’t provide information on tissue density or other thermal properties, which have to be found by special measurements. See Deuffhard et al. [6] for the successful application of CT imaging in a project of cancer therapy. Janssens, Thys, Clarys et al. [17], Romvari, Dobrowolski, Repa et al. [31], Allen, Branscheid, Dobrowolski [2] have a more skeptical view on such methods.

Individual anatomy can be acquired from a CT (computed tomography) scan of the corpse. The CT images have to be segmented into the different tissue types. For actual computation, a finite element mesh has to be created in such a way that a single tissue type can be assigned to each cell [36]. For a sample corpse, segmentation of CT data and mesh generation yield the tetrahedral mesh shown in Figure 2. Results of the simulation can be compared to those achieved on a coarse model developed by Mall et al. [22, 23]. We discuss this in the context of geometrical sensitivity in the next section.

In the CT-based model considered here we differentiate nine tissue types: bone, fat, muscle, gastrointestinal tract, bladder, kidneys, liver, heart, and lungs as shown in Figure 3. The corresponding mesh is composed of 1,439,552 tetrahedra, and 256,041 vertices.

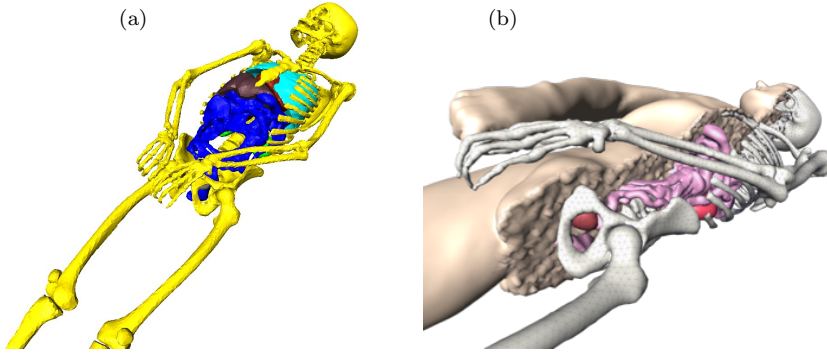


Fig. 3 (a) Skeleton and inner organs represented in the tetrahedral mesh of the corpse. Muscles, fat, and small intestine are not shown. (b) Illustration of tissues in the corpse including muscle, intestine, and fat.

Table 2 Averaged thermal properties of human tissues based on data from *ITIS Foundation*, [1]. The variation of muscle perfusion of $\pm 0.25 \text{ kg/s/m}^3$ given there applies to humans at rest. To account for physical activity before death, we assume a higher uncertainty of $\pm 0.50 \text{ kg/s/m}^3$ instead.

tissue	$\rho \pm \sigma_\rho$ kg/m^3	$c \pm \sigma_c$ J/kg/K	$\kappa \pm \sigma_\kappa$ W/m/K	$w \pm \sigma_w$ kg/s/m^3
fat	911 ± 53	2348 ± 372	0.21 ± 0.02	0.53 ± 0.21
bone	1543 ± 141	1794 ± 265	0.32 ± 0.03	0.48 ± 0.21
muscle	1090 ± 52	3421 ± 460	0.49 ± 0.04	0.71 ± 0.50
liver	1079 ± 53	3540 ± 119	0.52 ± 0.03	16.24 ± 3.21
intestine	1045 ± 50	3801 ± 300	0.56 ± 0.05	0.0
kidneys	1066 ± 56	3763 ± 120	0.53 ± 0.02	70.80 ± 10.15
urinary bladder	1000	3500	0.60	5.00 ± 0.50
heart	1050 ± 17	3617 ± 301	0.52 ± 0.03	183.8 ± 18.4
lungs	722 ± 87	3886 ± 300	0.39 ± 0.09	5.07 ± 4.72

Model parameters. The parameters entering into equations (1), (3), and (4) depend on the individual corpse and the environmental conditions at the supposed crime scene. Assigning specific values a priori is therefore subject to some uncertainty.

Thermal properties of different tissues have been extracted from the literature [8, 19, 22, 23]. From these, admittedly small, samples, average values and ranges have been computed, see Table 2. With all due caution, we interpret these values as mean and standard deviation of approximately log-normally distributed parameters. The combined parameter of heat capacity is again log-normally distributed with mean ρc and variance $\sigma_{\rho c}^2 = \sigma_\rho^2 \sigma_c^2 + \rho^2 \sigma_c^2 + c^2 \sigma_\rho^2$.

Similarly, the specific heat capacity c_b of blood has been obtained from literature. The well-known temperature dependence of the tissues' thermal properties [19] is assumed to be relatively small in the temperature range considered here, and is subsumed into the general variation. Only for the perfusion of muscle it seems to be appropriate to assume a higher standard deviation than mentioned in the *ITIS* database, in particular due to potential physical stress right before death [13].

While the uncertainty in tissue properties is due to moderate inter-individual differences and measurement errors, the effective heat transfer coefficient γ and the environmental temperature ϑ_{env} depend on the situation at the place of discovery, in particular

Table 3 Global parameters.

parameter	symbol	value	unit
heat capacity of blood	c_b	3617 ± 301	J/kg/K
body core temperature	ϑ_{core}	310.15 ± 0.50	K
environmental temperature	ϑ_{env}	297.15	K
environmental temperature rate	$\dot{\vartheta}_{\text{env}}$	0.00 ± 0.36	K/h
skin emissivity	ϵ	0.95 ± 0.05	
heat transfer coefficient	h	3.30 ± 0.30	W/m ² /K
effective heat transfer coefficient	γ	8.95 ± 0.60	W/m ² /K
supravital heat generation	Q_0	320 ± 160	W/m ³

on clothing and posture of the corpse, weather conditions, and underground. While the heat transfer coefficient h can, in principle, be measured, obtaining accurate values is virtually impossible in practice, since it is usually spatially varying and depends not only on the type of clothing but also on its drapery, its potential humidity penetration, the contact pressure at the surface supporting the corpse, and the shape of the body. The emissivity ϵ , too, depends on clothing. In contrast, variations due to air speed and posture can be taken easier into account [4]. In the end, the boundary condition parameter γ appears to be among the least precisely known, and the standard deviation assumed here is not more than an educated guess.

The environmental temperature is measured at the same time as the rectal temperature is acquired, but may have changed between the time of death and the measurement. This time course of ϑ_{env} is, to some extent, principally unknown, and again, the range merely a guess. For simplicity, we consider a single, spatially constant heat transfer coefficient $\gamma \in \mathbb{R}$ and a linear environmental temperature change, i.e.

$$\vartheta_{\text{env}}(t) = \vartheta_{\text{env}}(t_*) + (t_* - t)\dot{\vartheta}_{\text{env}}. \quad (5)$$

Note that the temperature value at t_* can be measured and is therefore assumed to be exactly known. The restriction to a linear temperature evolution model is not a severe limitation, as higher frequencies of the temperature will cancel out during the integration.

The amount of supravital heat generation is not particularly well known. For its value Q_0 at time of death we assume average of the values cited in [24, 34, 35], i.e. 320 Wm⁻³. This corresponds to authors supposing a value of similar magnitude as the heat generation in a resting healthy person, e.g., [18, 24, 32]. However, vastly different values have been reported in the literature [9, 11, 15, 16, 21, 22, 24, 26, 34], such that we assume a relatively large standard deviation of 50%.

With the three parameters ρc , κ , and w for each of the nine tissue types, and the global parameters ϑ_{core} , $\dot{\vartheta}_{\text{env}}$, γ , and Q_0 , in total $n_p = 31$ thermal parameters are considered here, and are for notational brevity referred to as the parameter vector $p \in \mathbb{R}^{n_p}$.

Finite element simulation. Given a mesh of the corpse's geometry (including tissue labels per element) and the vector p of all thermal parameters, the heat transfer model can be solved numerically for the temperature distribution $\vartheta(t; p)$ by the finite element method, see, e.g., [7, 37]. For the current work, we use the research code Kaskade 7 [12]. The simulation provides a complete temperature distribution within the entire grid, from which cooling curves at particular measurement points can be extracted.

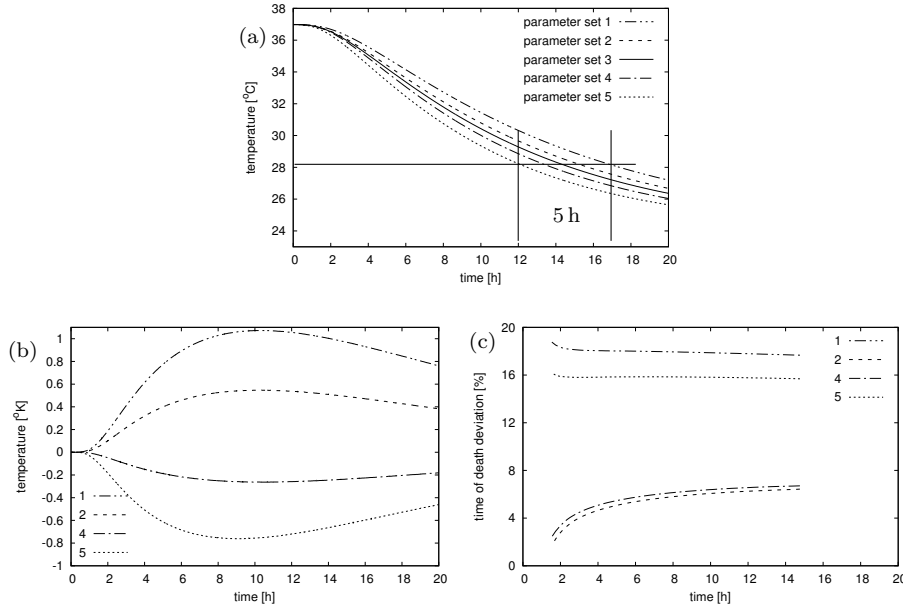


Fig. 4 Typical cooling of a node in a model region representing the rectum from FE simulations for five arbitrary parameter sets within the uncertainty ranges. (a) Cooling curves. (b) Difference between results based on parameter sets 1, 2, 4, and 5 and the cooling curve computed with the average values for the parameters (set 3). (c) Relative impact on time of death compared with the set 3 curve.

	bone		muscle		fat	
	c	κ	c	κ	c	κ
set 1	$+\sigma_c$	$-\sigma_\kappa$	$+\sigma_c$	$-\sigma_\kappa$	$+\sigma_c$	$-\sigma_\kappa$
set 2	$+\sigma_c$	$+\sigma_\kappa$	$+\sigma_c$	$+\sigma_\kappa$	$+\sigma_c$	$+\sigma_\kappa$
set 3	0	0	0	0	0	0
set 4	$-\sigma_c$	$-\sigma_\kappa$	$-\sigma_c$	$-\sigma_\kappa$	$-\sigma_c$	$-\sigma_\kappa$
set 5	$-\sigma_c$	$+\sigma_\kappa$	$-\sigma_c$	$+\sigma_\kappa$	$-\sigma_c$	$+\sigma_\kappa$

Table 4 Parameter sets used for the deviations shown in Figure 4. Set 3 uses the mean values from Table 2, whereas the other tissue properties are changed within the range of assumed standard deviation. Due to the sign structure, set 1 and set 5 are the extreme cases.

The uncertainty in the thermal and environmental parameters translates into a corresponding uncertainty in the cooling process and ultimately the ToD estimate. For illustration, five cooling curves have been computed based on a combination of lower and upper deviations for heat conductivity κ and specific heat capacity c in fat, muscle, and bone as given in Table 4. Let us point out that this illustration is optimistic, as uncertainties in environmental conditions are neglected. The results in Figure 4 (a), show that there can be a difference of up to five hours in the estimated ToD. Compared to the center curve of parameter set 3, the uncertainty range is still up to two and a half hour. Despite these significant deviations in ToD estimates in the range of 30%, the deviation of the cooling curves themselves is visually small. For that reason, we rather plot the temperature differences as shown in Figure 4 (b). The differences vary strongly

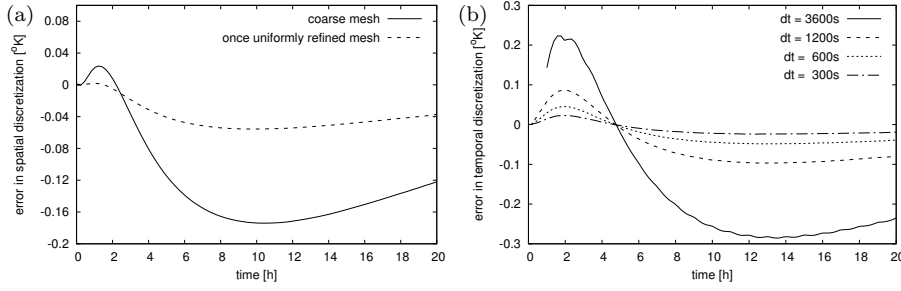


Fig. 5 Temperature prediction error in rectal point due to numerical discretization errors for a 20h cooling period. (a) Errors for differently fine spatial discretization with linear finite elements. (b) Errors for different time step sizes of a linearly implicit Euler scheme.

with the time of death, and moreover one is interested in the estimated time of death t_* rather than the temperature curve $\vartheta(t; p)$. Thus, in Figure 4 (c), we plot the relative deviation of the estimated time of death, i.e. $|\delta t|/t_*$ with $\delta t = \vartheta^{-1}(\vartheta_m; p) - t_*$. Except for very short times, the relative deviation is quite independent of t_* , and should be suitable as a quantity of interest to measure the parameter impact.

The discretization of the domain introduces both, a numerical discretization error and a geometric approximation error due to the assignment of tissue types to cells. The numerical discretization error can exceed the error due to parameter variation. In Figure 5, errors due to spatial and temporal discretization with different resolution are shown. Three levels of uniform mesh refinement (each of them dividing each of the given tetrahedra into eight new ones using the midpoints of the edges on the coarse grid as new points) have been used in Figure 5 (a) where the finest grid is assumed to provide accurate values and the deviation of the coarser meshes with respect to that reference is shown. On the right, results from different time step sizes (3600s, 1200s, 600s and 300s) are compared against a more accurate integration.

Fortunately, discretization errors can be kept below any prescribed tolerance by error estimation used for adaptive mesh refinement and time step selection, respectively, during the solution process [7]. For all simulations presented here we used linear finite elements and an extrapolated linearly implicit Euler time stepping scheme of order three, and made sure that the numerical discretization error is well below any of the considered modeling errors.

In contrast, the geometric approximation error is determined once by geometry reconstruction, depending on the voxel size of the medical image data as well as a curvature dependent limit (error quadratics) while coarsening the thereof reconstructed triangulation [10]. Its impact on the estimated ToD is investigated in the subsequent Section 4.

3 Impact of Thermal Parameter Uncertainty

In this section, we systematically investigate the impact of parameter uncertainty on the ToD estimate. The aim is to identify those parameters which need special attention as their uncertainty from literature values affects the ToD estimate most. These

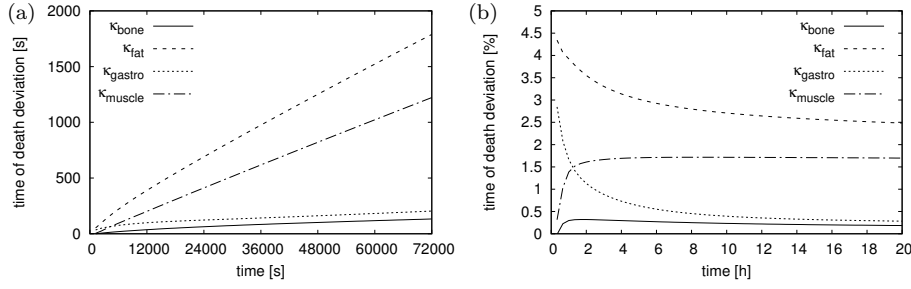


Fig. 6 Expected magnitude of ToD estimate deviation due to uncertainty in tissue heat conductivity. (a) Absolute deviation $|\delta t|$. (b) Relative deviation $|\delta t|/\bar{t}$ for tissue heat conductivity κ .

parameters can then be measured directly or included in a more complex estimate procedure in order to improve the accuracy of the MA result.

Sensitivities. Let us assume that a rectal temperature ϑ_m has been measured, and that the physical reality is described by the parameter vector p_* . The exact ToD is then the value t_* satisfying

$$\vartheta(t_*; p_*) = \vartheta_m.$$

Of course, p_* is not accurately known, and the simulation is performed with an approximation $\bar{p} = p_* + \delta p$, e.g., the mean values from the previous section. The ToD estimate $\bar{t} = t_* + \delta t$ satisfies

$$\vartheta(\bar{t}; \bar{p}) = \vartheta_m. \quad (6)$$

Assuming the parameter deviation δp to be sufficiently small, the implicit function theorem yields

$$\delta t \approx S(\bar{t})^T \delta p = \sum_{i=1}^{n_p} S_i(\bar{t}) \delta p_i, \quad (7)$$

with the sensitivity

$$S(\bar{t}) := -\frac{\partial_p \vartheta(\bar{t}; \bar{p})}{\partial_t \vartheta(\bar{t}; \bar{p})} \in \mathbb{R}^{n_p}, \quad (8)$$

where ∂_p and ∂_t denote the respective partial derivative. The individual sensitivities S_i can be computed by evaluation of the derivatives of ϑ either by numerical differentiation or, more accurately, by solving the tangent equations. The latter method has been used to provide the sensitivity values reported here. Of greater interest than the sensitivities themselves is of course the impact on the ToD estimate. The error δt depends on the parameter deviation δp , such that we focus on sensitivities scaled by the parameter uncertainty, i.e. $|S_i(\bar{t}) \sigma_{p_i}|$. In contrast, the sensitivity study [33] judges the influence of parameter changes on the ToD estimate only in terms of relative parameter change.

As illustrated in Figure 6, these quantities vary significantly with \bar{t} and are therefore unintuitive to compare for different parameters. We consider the relative error $\delta t/\bar{t}$ of ToD estimation instead and compare the individual impact values

$$I_{p_i}(\bar{t}) := \bar{t}^{-1} |S_i(\bar{t}) \sigma_{p_i}|, \quad (9)$$

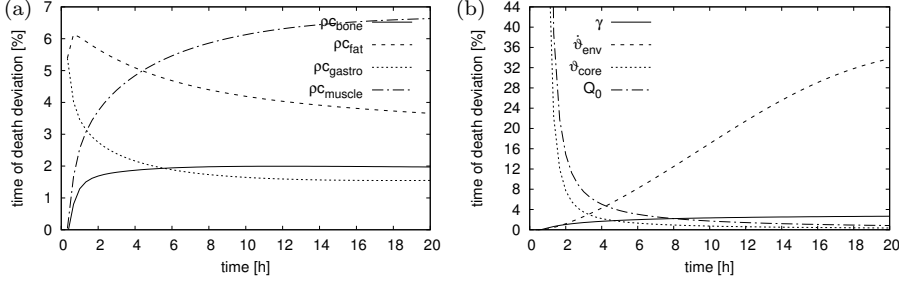


Fig. 7 Parameter uncertainty impact $I_{p_i}(\bar{t})$ (a) for tissue heat capacity ρc . (b) for the global parameters environmental temperature rate $\dot{\vartheta}$, initial core temperature $\dot{\vartheta}_{core}$, the effective heat transfer coefficient γ , and the supravitral heating by metabolism Q .

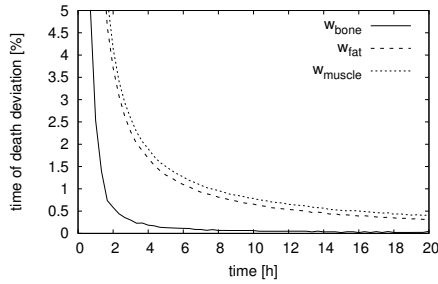


Fig. 8 Parameter uncertainty impact $I_p(\bar{t})$ for tissue perfusion w .

which depend much less on \bar{t} except for small \bar{t} . In Figures 6 – 7, these values are shown for tissue parameters κ , ρc , and the global parameters from Table 3, respectively. Only the few largest values are shown in order not to clutter the plots and because the values for the other parameters are less than 0.1%.

As a single number quantifying the impact of uncertainty in a parameter p_i we define I_{p_i} as the median of $I_{p_i}(\bar{t})$ over the interval $\bar{t} \in]0, 20]$ h. Since most relative sensitivity curves are almost monotone, this is essentially the value for $\bar{t} = 10$ h.

Stochastic interpretation. Let us interpret $\delta p \in \mathbb{R}^{n_p}$ as a random variable with components δp_i . For lack of more precise information, we assume δp_i to be uncorrelated, have mean zero, and a standard deviation σ_{p_i} as provided by the uncertainty ranges in Tables 2 and 3. Then, by eq. (7), $\delta t(\bar{t})/\bar{t} \in \mathbb{R}$ is a random variable with mean $E[\delta t] \approx 0$ and variance

$$\sigma_{\delta t/\bar{t}}(\bar{t})^2 \approx \sum_{i=1}^{n_p} \frac{S_i(\bar{t})^2}{\bar{t}^2} \sigma_{p_i}^2 = \sum_{i=1}^{n_p} I_{p_i}(\bar{t})^2. \quad (10)$$

The importance of reducing a parameter uncertainty by a certain fraction $r_i < 1$ from σ_{p_i} to $r_i \sigma_{p_i}$ can be quantified by the improvement of the ToD estimate standard deviation in terms of its derivative

$$\hat{I}_{p_i}(\bar{t}) := \left. \frac{\partial \sigma_{\delta t/\bar{t}}(\bar{t})}{\partial r_i} \right|_{r_i=1} = \frac{S_i(\bar{t})^2 \sigma_{p_i}^2}{\bar{t}^2 \sigma_{\delta t/\bar{t}}(\bar{t})} = \frac{I_{p_i}(\bar{t})^2}{\sigma_{\delta t/\bar{t}}(\bar{t})}. \quad (11)$$

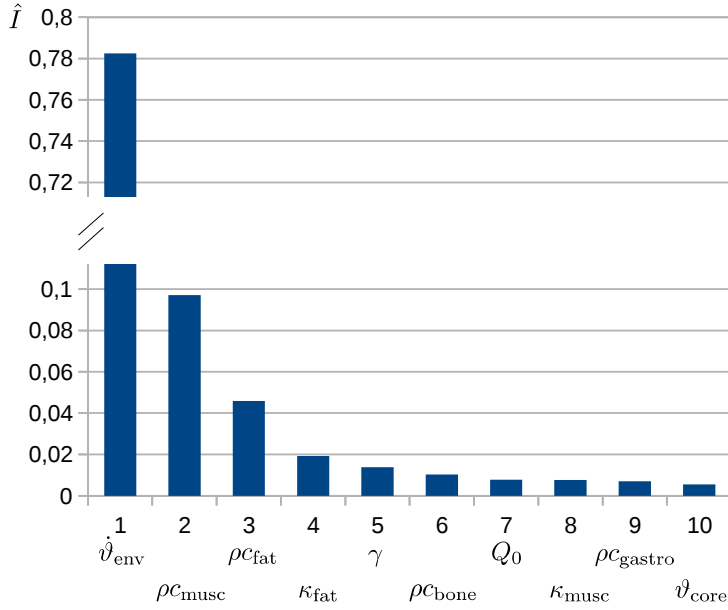


Fig. 9 Thermal parameters p_i sorted by their importance \hat{I}_{p_i} according to (11).

In contrast, the impact value $I_{p_i}(\bar{t})$ itself describes the derivative with respect to a relative uncertainty reduction by r_i if p_i is the only uncertain parameter.

Again, we define \hat{I}_{p_i} as the median over $\bar{t} \in [0, 20]$ h and observe that usually $\hat{I}_{p_i} \approx I_{p_i}^2 / \sigma_{\delta t} / \bar{t} (10\text{h})$ holds. Ordering the parameters according to their contribution to ToD estimate uncertainty is therefore almost independent of whether I_{p_i} or \hat{I}_{p_i} is considered, but their relative importance is different, with \hat{I}_{p_i} putting more weight on the least certain parameters. The values of \hat{I}_{p_i} are shown in Figure 9. Note, however, that the parameter uncertainties σ_{p_i} enter directly into the values of \hat{I}_{p_i} , affecting their relative importance. As these uncertainties are not particularly well-known themselves, but for some parameters merely educated guesses, the comparison is more of a qualitative nature.

Discussion. The relative ToD estimate uncertainty due to uncertainties in thermal parameters amounts to 20% according to (10), based on the very rough estimates of parameter uncertainty from Tables 2 and 3. This value amounts to two hours of estimation error for a ToD of about 10 h and underlines the need for more accurate estimation. Improving the accuracy requires to reduce the parameter uncertainty by including additional information, e.g., further temperature measurements or experimental quantification of parameters.

According to Figure 9, the most important parameter to characterize more accurately is the rate \dot{v} of environmental temperature change since the time of death, even though the assumed uncertainty range of 0.36 K/h is in no way exaggerated. That parameter alone can lead to 10–20% estimation error and more. This observation is in agreement with the findings of [33], where environmental and initial temperature

have been identified as most influential parameters. On the one hand, the large impact of environmental temperature rate is unfortunate, since the temperatures cannot be measured retrospectively. On the other hand, additional information from weather recordings or heating control may be available and reduce the uncertainty. If the course of the external temperature is known exactly, the remaining parameter uncertainties induce a relative ToD standard deviation of 9.1%, almost an hour error for a ToD of about 10 h. Assuming a constant environmental temperature in case of lacking information, however, is bound to introduce rather large estimation errors.

The remaining parameters all incur much less uncertainty. Heat capacities ρc of muscle and fatty tissue have an individual impact on the estimation error of about 4–6%. In general, heat capacity has a slightly larger impact than heat conductivity. The dominance of muscle and fat properties is simply due to their large volume in the vicinity of the rectal measurement point. While in principle the heat capacity of tissue can be measured, unknown spatial variability of the heat capacity, difficulties of obtaining samples, and the nontrivial measurement itself make this approach problematic in forensic practice.

Also of some importance are the heat transfer coefficient γ and the heat conductivity κ of fatty tissue. Less impact have the initial body core temperature ϑ_{core} , supravital heat generation amplitude Q_0 , thermal properties of bones and the gastrointestinal tract, and muscle and fat perfusion. Initial body core temperature has been found to be one of the two most influential parameters in [33]. The apparent difference in findings is by reason of the small standard deviation $\sigma_{\vartheta_{\text{core}}} = 0.5 \text{ K}$ that we assume, which amounts to a relative deviation (with respect to 0°C) of only 1.3%. The uncertainty in ϑ_{core} has a particularly large impact during the first few hours of cooling. This is due to the fact that in the BHTE (4), it directly affects the initial temperature at the rectal measurement point. Together with the vanishing time derivative in the initial plateau phase, this leads to a large ToD estimation uncertainty. A similar effect has the supravital heat generation during the first few hours. Much smaller is the impact of fat and tissue perfusion, which also affect the initial temperature at the measurement location.

The uncertainty of the remaining thermal tissue parameters has a negligible impact on the ToD estimate. These are in particular the tissue properties of heart, lungs, liver, kidneys, and urinary bladder. The reason is, that on one hand most of these organs are far away from the rectal measurement point, and on the other hand their volume and hence total heat capacity is small compared to muscle and fat tissues. This minor impact indicates that an explicit representation of these organs might not be necessary at all, which would simplify geometry acquisition, segmentation, and meshing.

4 Geometry Representation

Besides the thermal material parameters, the corpse geometry and the spatial distribution of different tissues and organs might play a decisive role. In this section we investigate the impact of geometric representation of the corpse on the estimated ToD. Of course, geometry representation is neither a scalar nor a continuous parameter, for which reason the derivative-based approach of the previous section is inapplicable. Instead, we use the highly resolved geometry of the corpse as illustrated in Figures 2 and 3 as a reference, which in turn provides a reference ToD estimate. Then, several coarser representations as shown in Figure 10 are created as follows. The skin surface triangu-

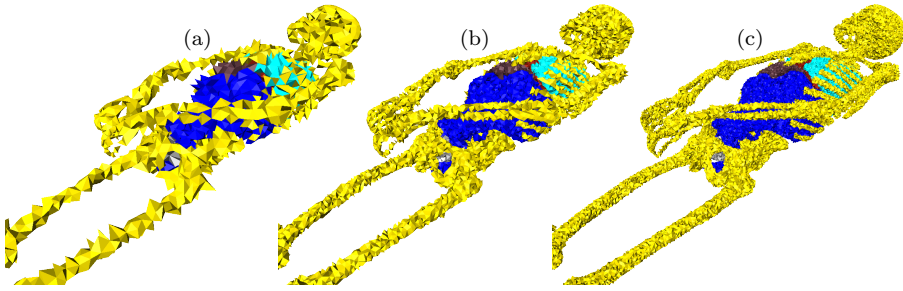


Fig. 10 Three levels of resolution of the the corpse: (a) 7066, (b) 65769, and (c) 326914 vertices.

lation is coarsened [10] and remeshed with respect to triangle quality [38]. The resulting triangulation is then filled with tetrahedra using an advancing front approach [20, 28], since this is particularly suited for domains with complicated boundaries and internal interfaces. Advancing front techniques belong to the class of heuristic mesh generation methods. The name refers to the strategy of generating elements successively from an ever shrinking set of dynamic surfaces that starts at the boundaries and internal interfaces of the domain and advances into its interior. The generation of tetrahedral meshes of different resolutions for a grid independence study does not take any internal tissue boundaries into account. Our mesh generator offers a gradation from small to large element sizes and vice versa, starting with the given resolution of the boundary surface that can either be increased or decreased within a certain limit (e.g., by a small percentage of the actual element size) [3]. Finally, each cell of the resulting meshes is labeled with a tissue type according to the largest volume fraction of tissue within that cell. The volume fraction is directly taken from the segmentation respectively the original image data. While the tissue boundaries and hence their volume fractions are not retained, the total heat capacity of the body differed only by less than 1% from the reference anatomy.

Deviations of simulated cooling curves from the reference are interpreted as resolution-dependent errors. For the cooling simulations we therefore made sure that the numerical discretization error of the temperature distribution is small compared to the error due to coarse anatomy resolution by applying grid refinement to the coarse models. Thus, the reported deviation is only due to the geometrical resolution of the tissue distribution. In the same way, the numerical temperature discretization error has been assessed for Figure 5 (a): The anatomy and tissue distribution was always the coarse 7k mesh, and different discretization errors are obtained by refining that grid for actual computation.

The differences of the cooling curves to the reference are shown in Figure 11 (a), for three different resolutions of the tissues in the corpse. Compared to the cooling curves for varying thermal parameters in Figure 4, the errors are smaller by a factor of ten even for the coarsest grid, and by a factor about 100 for the still coarse 65k mesh. The relative error in ToD estimation is shown in Figure 11 (b) and can be directly compared to Figures 6 and 7. Again, the effect of low geometric resolution is much smaller than that of the dominant thermal parameters.

There is no evidence for a significant sensitivity with respect to geometric resolution of tissue boundaries, even though the tissues may change the total heat capacity in

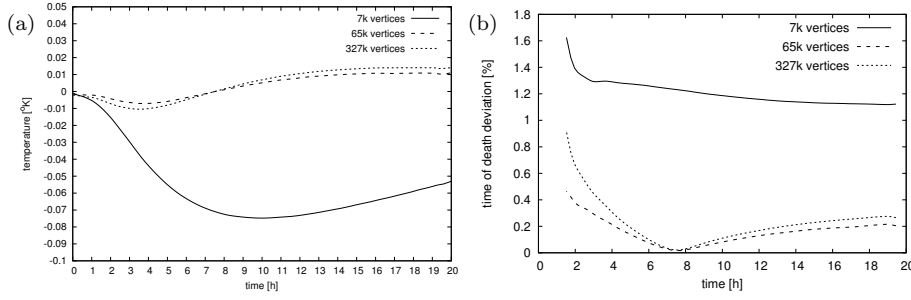


Fig. 11 Deviation of different levels of geometrical resolution from a solution on a highly resolved geometry. (a) Cooling curves. (b) Induced relative ToD estimation error.

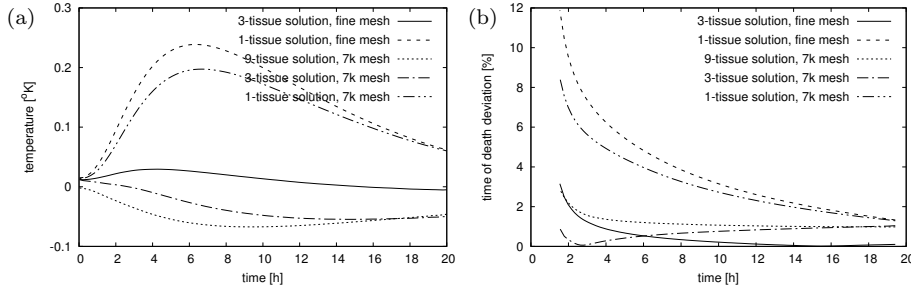


Fig. 12 Deviation of different levels of tissue differentiation from a solution on a detailed geometry. (a) Cooling curves. (b) Induced relative ToD estimation error.

the different tissue compartments as well as in the whole corpse. In particular, it can be concluded that there is no need for providing high resolution segmentation and meshing.

This insensitivity to the exact geometric differentiation of tissue types, together with the negligible impact of thermal properties of small organs, suggests that a rather coarse model might be sufficiently accurate. A moderate coarsening would subsume liver, intestine, kidneys, bladder, heart, and lungs under muscle tissue, and differentiate only fat, bone, and muscle-like tissues. In the extreme case, just a homogeneous body with suitably averaged thermal properties might be used. Indeed, a homogeneous model with cylindrical geometry has been proposed in [33]. Let V_{fat} , V_{bone} , and V_{muscle} denote the volume fractions of fat tissue, bones, and all water-dominated tissues, respectively, such that $V_{\text{fat}} + V_{\text{bone}} + V_{\text{muscle}} = 1$. Then the average properties of a homogeneous substitute are defined as

$$c\rho = \sum_{i \in \{\text{fat}, \text{bone}, \text{muscle}\}} V_i c\rho_i, \quad \kappa^{-1} = \sum_{i \in \{\text{fat}, \text{bone}, \text{muscle}\}} V_i \kappa_i^{-1}.$$

In the high-resolution model we get the average values $c\rho = 3.103e6$ and $\kappa = 0.3275$, and in the coarse 7k model $c\rho = 3.179e6$ and $\kappa = 0.3425$. The errors introduced by these simplifications are shown in Figure 12, and can be directly compared to Figure 11.

5 Conclusions

The sensitivity results clearly show that a highly accurate and detailed representation of individual anatomy is not necessary for the mechanistic approach to provide accurate time of death estimates. As long as the total volumes of tissues with dominant water or dominant fat composition and their overall geometric location are accurately captured, the geometric resolution has virtually no impact on the estimated ToD – at least as long as the temperature measurement is restricted to a single rectal location.

In contrast, some thermal parameters appear to play a crucial role, in particular the time course of the environmental temperature, but also heat capacity of muscle and fatty tissues, their heat conductivities, and the effective heat transfer coefficient. With uncertainty ranges from literature, a total uncertainty of about 20% in the ToD estimate from the simulation method is to be reckoned with for only one measurement, which calls for improved estimation methods. In this situation, multiple temperature measurements may provide the additional information that is necessary to increase the reliability of the estimation.

While the results are obtained on a single corpse geometry, and are therefore exemplary, we believe that the conclusions drawn from them are valid for a wide range of anatomies and environmental conditions. This, however, needs to be confirmed through further studies.

Acknowledgement. We thank our colleague Marian Moldenhauer for careful reading of the article and for helpful comments. Funding by the University of Jena is gratefully acknowledged.

Conflict of Interest: The authors declare that they have no conflict of interest.

References

1. Foundation for Research on Information Technologies in Society (IT²IS). Zurich, Switzerland.
2. P. Allen, W. Branscheid, A. Dobrowolski, and P. Horn. Schlachtkörperwertbestimmung beim Schwein - Röntgen-Computertomographie als mögliche Referenzmethode. *Fleischwirtschaft*, 3:109–112, 2004.
3. H. Borouchaki, F. Hecht, and P.J. Frey. Mesh gradation control. *Int. J. Numer. Meth. Eng.*, 43(6):1143–1165, 1998.
4. Y.A. Cengel and A.J. Ghajar. *Heat and Mass Transfer, Fundamentals & Applications*. MacGraw-Hill, 2015.
5. J.P. Clarys, S. Provyn, and M.J. Marfell-Jones. Cadaver studies and their impact on the understanding of human adiposity. *Ergonomics*, 48:1445–1461, 2005.
6. P. Deuffhard, A. Schiela, and M. Weiser. Mathematical cancer therapy planning in deep regional hyperthermia. *Acta Numerica*, 2:307–378, 2012.
7. P. Deuffhard and M. Weiser. *Adaptive numerical solution of PDEs*. de Gruyter, 2012.
8. P. Deuffhard, M. Weiser, and M. Seebaß. A new nonlinear elliptic multilevel FEM applied to regional hyperthermia. *Comput. Vis. Sci.*, 3(3):115–120, 2000.
9. D.C. Frankenfield, J.S. Smith Jr, R.N. Conney, S.A. Blosser, and G.Y. Sarson. Relative association of fever and injury with hypermetabolism in critically ill patients. *Injury*, 28(9–10):617–621, 1997.
10. M. Garland and P.M. Heckbert. Surface simplification using quadric error metrics. In *Proceedings of the 24th Annual Conference on Computer Graphics and Interactive Techniques, SIGGRAPH '97*, pages 209–216, 1997.
11. Hutchins G.M. Body temperature is elevated in the early postmortem period. *Human Pathology*, 16(6):560–561, 1985.

12. S. Götschel, M. Weiser, and A. Schiela. Solving optimal control problems with the Kaskade 7 finite element toolbox. In A. Dedner, B. Flemisch, and R. Klöfkor, editors, *Advances in DUNE*, pages 101–112. Springer, 2012.
13. A.C. Guyton and J.E. Hall. *Textbook of Medical Physiology*. Saunders, 2000.
14. C. Henßge. Death time estimation in case work. I: The rectal temperature time of death nomogram. *Forensic Sci. Int.*, 38:209–236, 1988.
15. C. Henßge and B. Madea. Estimation of the time since death in the early post-mortem period. *Forensic Sci. Int.*, 144:167–175, 2004.
16. P. Hooft and H. van de Voorde. The role of intestinal bacterial heat production in confounding postmortem temperature measurements. *Rechtsmedizin*, 102:331–336, 1989.
17. V. Janssens, P. Thys, J.P. Clarys, H. Kvis, B. Chowdhury, E. Zinzen, and J. Cabri. Post-mortem limitations of body composition analysis by computed tomography. *Ergonomics*, 37:207–216, 1994.
18. R. Klinke and S.A. Silbernagl, editors. *Lehrbuch der Physiologie*. Thieme, 1994.
19. J. Lang, B. Erdmann, and M. Seebaß. Impact of Nonlinear Heat Transfer on Temperature Control in Regional Hyperthermia. *IEEE Trans. Biomed. Eng.*, 46(9):1129–1138, 1999.
20. S.H. Lo. Automatic mesh generation over intersecting surfaces. *Int. J. Num. Meth. Eng.*, 38:943–954, 1995.
21. B. Madea. Importance of supravitality in forensic medicine. *Forensic Sci. Int.*, 69:221–241, 1994.
22. G. Mall and W. Eisenmenger. Estimation of time since death by heat-flow finite-element model. Part I: Method, model, calibration and validation. *Legal Medicine*, 7:1–14, 2005.
23. G. Mall and W. Eisenmenger. Estimation of time since death by heat-flow finite-element model. Part II: Application to non-standard cooling conditions and preliminary results in practical casework. *Legal Medicine*, 7:69–80, 2005.
24. G. Mall, M. Hubig, G. Beier, A. Büttner, and W. Eisenmenger. Supravital energy production in early post-mortem phase – Estimate based on heat loss due to radiation and natural convection. *Legal Medicine*, 4:71–78, 2002.
25. T. Marshall and F. Hoare. Estimating the time of death: The rectal cooling after death and its mathematical expression. *J. Forensic Sci.*, 7:56–81, 1962.
26. H. Muggenthaler, I. Sinicina, M. Hubig, and G. Mall. Database of post-mortem rectal cooling cases under strictly controlled conditions: A useful tool in death time estimation. *Legal Medicine*, 126:79–87, 2012.
27. H.H. Pennes. Analysis of tissue and arterial blood temperatures in the resting human forearm. *J. Appl. Phys.*, 1:93–122, 1948.
28. A. Rassinoux. Generation and optimization of tetrahedral meshes by advancing front technique. *Numer. Meth. Eng.*, 41:651–674, 1998.
29. M.R. Rodrigo. Time of death estimation from temperature readings only: A Laplace transform approach. *Applied Mathematics Letters*, 39:47–52, 2014.
30. M.R. Rodrigo. A nonlinear least squares approach to time of death estimation via body cooling. *Forensic Sci.*, 61(1):230–233, 2016.
31. R. Romvari, A. Dobrowolski, and I. Repa. Development of a computed tomographic calibration method for the determination of lean meat content in pig carcasses. *Acta Vet. Hung.*, 54(1):1–10, 2006.
32. R.F. Schmidt, G. Thews, and F. Lang, editors. *Physiologie des Menschen*. Springer, 1997.
33. J. Smart. Estimation of time of death with a Fourier series unsteady-state heat transfer model. *J. Forensic Sci.*, 55(6):1481–1487, 2010.
34. J. Smart and M. Kaliszan. The post-mortem temperature plateau and its role in the estimation of time of death. A review. *Legal Medicine*, 14:55–62, 2012.
35. J. Werner. *Regelung der menschlichen Körpertemperatur*. de Gruyter, 1984.
36. S. Zachow, M. Zilske, and H.-C. Hege. 3d reconstruction of individual anatomy from medical image data: Segmentation and geometry processing. In *25. ANSYS Conference & CADFEM Users’ Meeting*, 2007.
37. O. Zienkiewicz, R.L. Taylor, J.Z. Zhu, and Nithiarasu P. *The finite element method*. Elsevier Butterworth-Heinemann, 2005.
38. Michael Zilske, Hans Lamecker, and Stefan Zachow. Adaptive remeshing of non-manifold surfaces. In *Eurographics 2008 Annex to the Conf. Proc.*, pages 207 – 211, 2008.